Electronic supplementary information

Boosting bifunctional oxygen electrocatalysis by integrating Fe-N_x moieties and FeNi nanoparticles for highly efficient and long-life rechargeable zinc-air batteries

Zubair Ahmed[a], Jekaterina Kozlova[b], Kaupo Kukli[b], Arvo Kikas[b], Vambola Kisand[b], Alexey Treshchalov[b], Maike Käärik[a], Jaan Leis[a], Jaan Aruväli[c], and Kaido Tammeveski[a,*]

[a]*Institute of Chemistry, University of Tartu, Ravila 14a, 50411 Tartu, Estonia*

[b]*Institute of Physics, University of Tartu, W. Ostwald Str. 1, 50411 Tartu, Estonia*

[c]*Institute of Ecology and Earth Sciences, University of Tartu, Vanemuise 46, 51014 Tartu, Estonia*

*Corresponding author, E-mail address: kaido.tammeveski@ut.ee (K. Tammeveski)

1. Koutecky-Levich analysis

The ORR polarization curves at different rotation rates were recorded at a scan rate (ν) of 10 mV s^{-1} with the electrode rotation rates (ω) from 600 to 3000 rpm. The electron transfer number (n) was calculated from the Koutecky-Levich (K-L) equation [1]:

$$j^{-1} = j_k^{-1} + B^{-1}\omega^{-1/2} \tag{S1}$$

$$j_k = \mathrm{nF}kC_O \tag{S2}$$

$$B = 0.62\mathrm{nF}C_0D_0^{2/3}\upsilon^{-1/6} \tag{S3}$$

where j and j_k represent the experimental and kinetic current densities at a specific potential, j_d is the diffusion-limited current density, n is the number of electrons transferred per O_2 molecule, k is the O_2 reduction rate constant at a specific potential (cm s^{-1}), F is the Faraday constant (96485 C mol^{-1}), D_O is the O_2 diffusion coefficient in 0.1 M KOH (1.9×10^{-5} cm^2 s^{-1}), ν is the kinematic viscosity of the electrolyte solution (0.01 cm^2 s^{-1}), C_O is the concentration of O_2 in the bulk solution (1.2×10^{-6} mol cm^{-3}), and ω is the electrode rotation rate (rad s^{-1}) [2].

2. Zn-air battery tests

Zn-air batteries performance were evaluated at ambient conditions without additional oxygen supply. The polarization curves and galvanostatic discharge–charge cycling curves were recorded by linear sweep voltammetry and CP-Chronopotentiometry, respectively. The specific capacity and round trip efficiency were calculated according to the equation as follows:

$$Specific\ capacity = \frac{current \times service\ hours}{weight\ of\ consumed\ zinc}$$

(S4)

$$Round\ trip\ efficiency\ (\varepsilon) = \frac{E_{discharge}}{E_{charge}} \times 100\%$$

(S5)

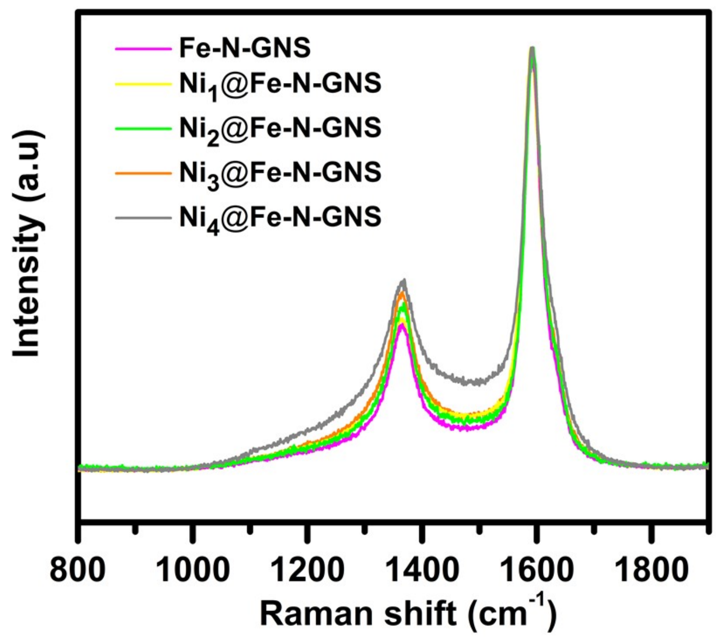

Fig. S1. Raman spectra of the prepared Fe-N-GNS, Ni_1@Fe-N-GNS, Ni_2@Fe-N-GNS, Ni_3@Fe-N-GNS, and Ni_4@Fe-N-GNS catalyst materials.

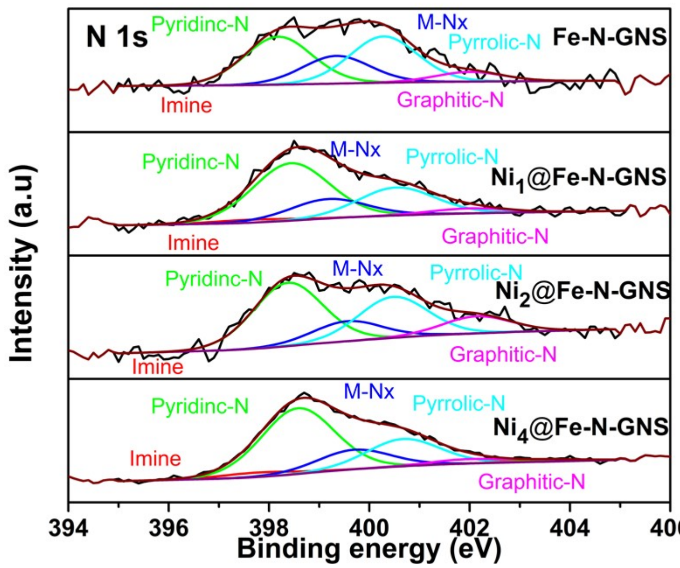

Fig. S2. The high-resolution XPS spectra of N 1s for Fe-N-GNS, Ni_1@Fe-N-GNS, Ni_2@Fe-N-GNS, and Ni_4@Fe-N-GNS catalyst materials.

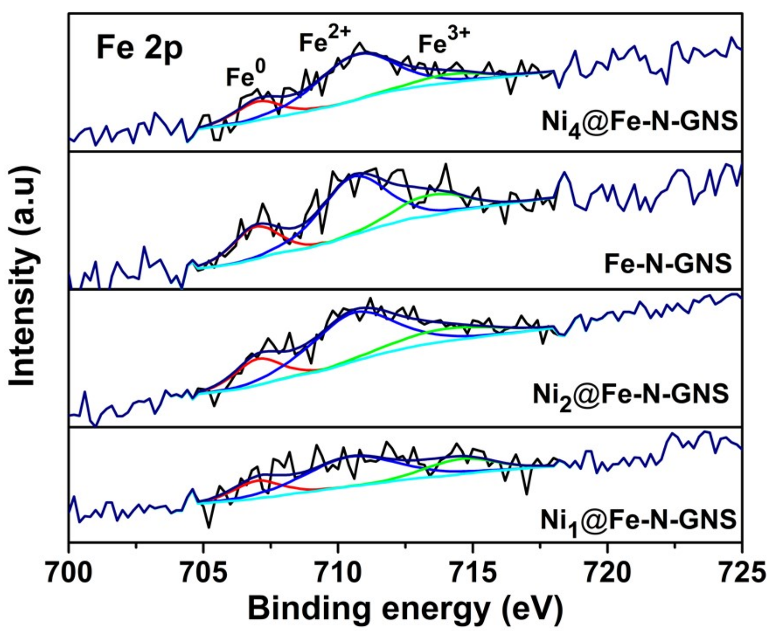

Fig. S3. The high-resolution XPS spectra of Fe 2p for Fe-N-GNS, Ni_1@Fe-N-GNS, Ni_2@Fe-N-GNS, and Ni_4@Fe-N-GNS catalyst materials.

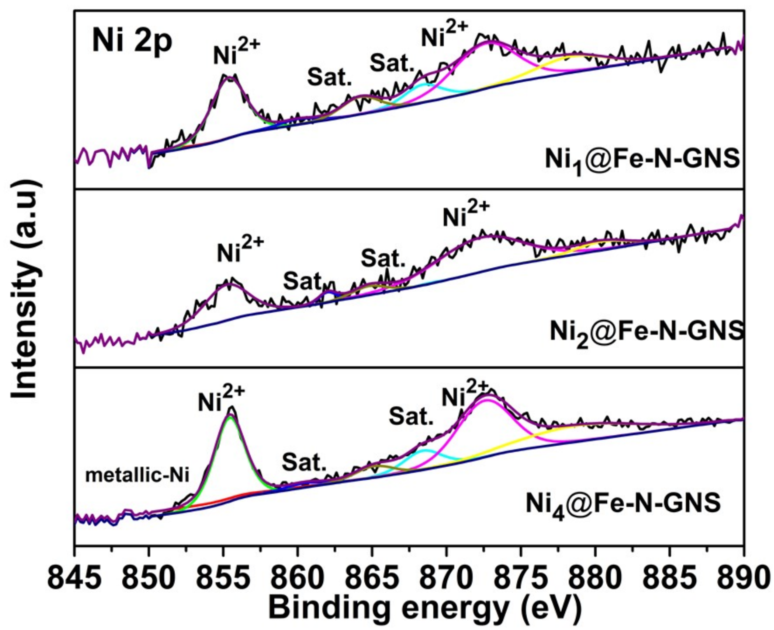

Fig. S4. The high-resolution XPS spectra of Ni 2p for Fe-N-GNS, Ni_1@Fe-N-GNS, Ni_2@Fe-N-GNS, and Ni_4@Fe-N-GNS catalyst materials.

Table S1: Composition percentage analysis by Rietveld refinement of all the catalysts.

	Fe-N-GNS	Ni_1@Fe-N-GNS	Ni_2@Fe-N-GNS	Ni_3@Fe-N-GNS	Ni_4@Fe-N-GNS
Carbon	96.4	96.18	93.8	93.11	93.85
Fe_3C	1.3	0.95	0.93	0	0
Fe	0.8	0.2	0	0	0
Fe_3O_4	1.5	0.63	0.90	0.47	0.27
FeNi	0	2.04	4.43	6.42	5.88

Table S2. The surface elemental composition of the prepared catalysts by XPS analysis.

Element	**Functional form**	Fe-N-GNS		Ni_1@Fe-N-GNS		Ni_2@Fe-N-GNS		Ni_3@Fe-N-GNS		Ni_4@Fe-N-GNS	
		BE (eV)	at. %	BE (eV)	at.%	BE (eV)	at.%	BE (eV)	at.%	BE (eV)	at.%
C	sp^2	284.4	76.2	284.4	77.37	284.4	76.66	284.4	74.97	284.4	70.48
	sp^3	285.1	0	285	0	285.1	0.01	285	0	285.1	2.73
	C-O	286.3	4.05	286.3	3.04	286.3	3.93	286.3	3.2	286.3	4.71
	C=O	287.4	0.23	287.4	1.31	287.4	0.56	287.4	1.2	287.4	0.45
	O-C=O	288.3	3.8	288.3	1.19	288.3	3.39	288.3	2.29	288.3	3.74

	π-π*	290.4	5.15	289.9	5.21	290.4	5.48	290.2	5.14	290.4	5.47
	Carbide	283	3.14	283	2.71	282.8	2.63	283	3.74	282.7	2.09
	π-π*	295.5	3.43	292.5	3.52	292.1	3.52	292.3	3.94	292.7	3.28
N	Imine	397.4	0	397.9	0.09	397.6	0	397.8	0.08	397.6	0.03
	Pyridinic	398.2	0.22	398.7	0.2	398.4	0.35	398.6	1.22	398.4	0.53
	$M-N_x$	399.3	0.13	399.7	0.2	399.5	0.11	399.7	0.36	399.2	0.18
	Pyrrolic	400.3	0.21	400.8	0.15	400.5	0.23	400.7	0.51	400.5	0.26
	Graphitic	402	0.04	402	0.01	402.1	0.09	402	0.08	402.0	0.05
O	Metal oxide	530.1	0.38	530.2	0.42	530.2	0.52	530.3	0.5	530.1	0.26
	O=C-OH	531.2	0.54	531.2	0.7	531.2	0.4	531.2	0.84	531.2	0.8
	C=O carbonyl	531.7	0.57	531.7	1.26	531.6	0.5	531.9	0.78	531.3	0.33
	C-O	532.9	1.39	532.9	2.21	532.9	0.96	532.9	1.17	532.9	1.77
	C-OH	533.7	0.06	533.7	0.06	533.7	0.06	533.7	0.06	533.7	0.06
	Water, chemisorbed O	535.4	0.34	535.4	0.37	535.8	0.15	535	0.37	535	0.45
total Fe (at.%)	0.14			0.10		0.17		0.14		0.12	
total Ni (at.%)	0			0.21		0.27		0.35		0.97	
total N (at.%)	0.6			0.65		0.78		2.29		1.05	

Table S3. Elemental composition of as-prepared materials by SEM-EDX (wt.%).

Catalyst	C	N	O	Fe	Ni
Fe-N-GNS	87.56	3.78	4.18	4.48	0
Ni_3@Fe-N-GNS	83.82	3.8	2.84	4.68	4.86
Ni_4@Fe-N-GNS	83.53	5.56	4.19	4.93	6.90

Table S4. BET surface area (S_{BET}), volume of micropores (V_{micro}), total pore volume (V_{tot}), DFT surface area of micropores and mesopores calculated for Fe-N-GNS, Ni_3@Fe-N-GNS, and Ni_4@Fe-N-GNS catalysts

Catalyst	S_{BET} (m^2/g)	V_{tot} (cm^3/g)	S_{DFT} (m^2/g)	S_{DFT} micro (m^2/g)	S_{DFT} meso (m^2/g)	V_{micro} (cm^3/g)
Fe-N-GNS	394	0.71	341	140	201	0.08
Ni_3@Fe-N-GNS	352	0.56	328	180	148	0.08
Ni_4@Fe-N-GNS	300	0.52	264	130	134	0.07

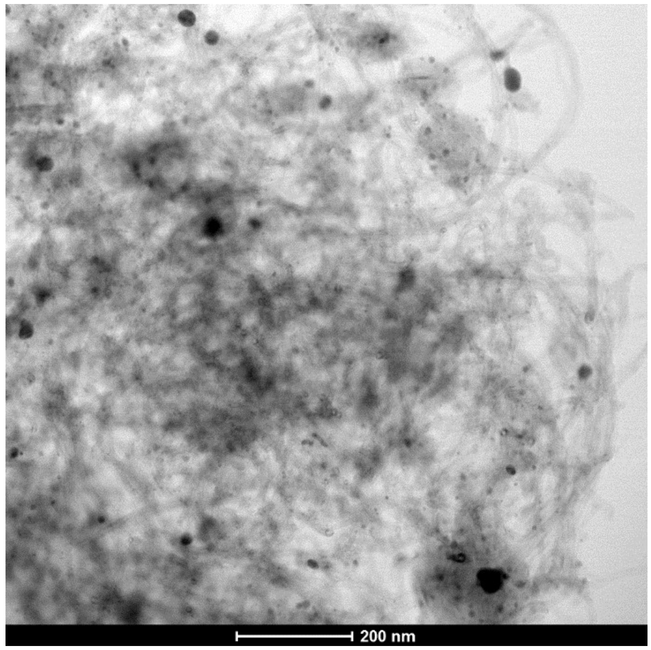

Fig. S5. BF-STEM image of the as-prepared Ni_3@Fe-N-GNS catalyst.

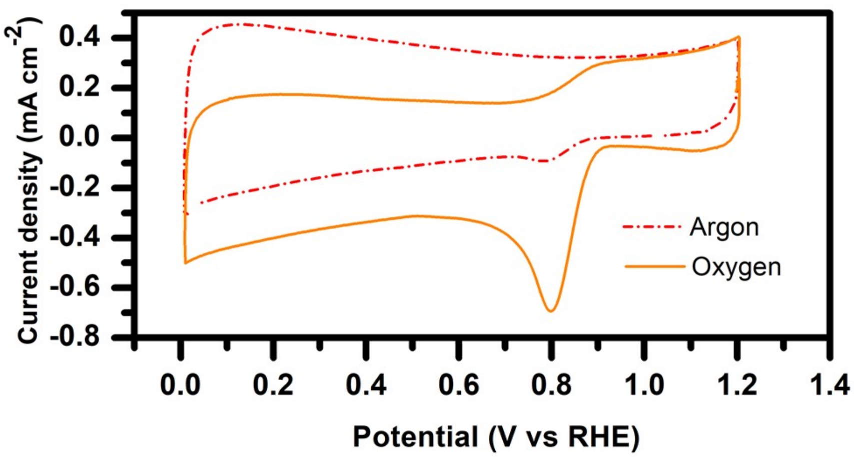

Fig. S6. CV curves of a Ni_3@Fe-N-GNS catalyst in O_2 and Ar saturated 0.1 M KOH solution (50 mV s^{-1}).

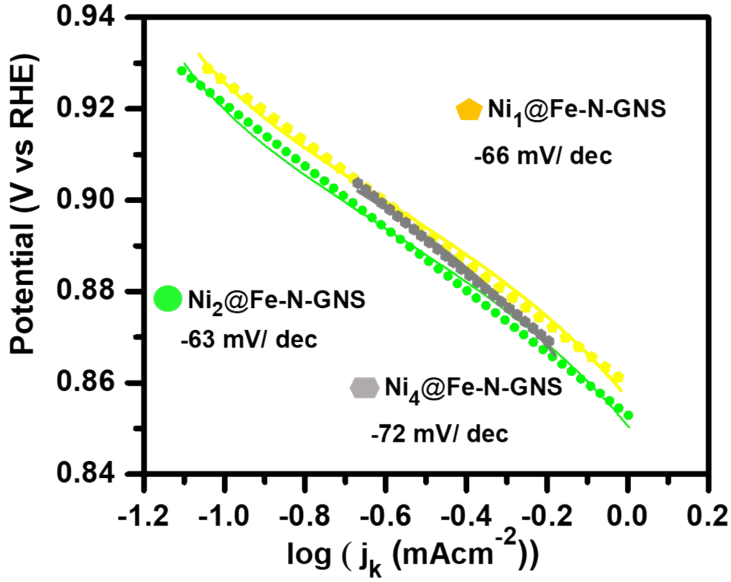

Fig. S7. Tafel plots for ORR on the Ni_1@Fe-N-GNS, Ni_2@Fe-N-GNS, and Ni_4@Fe-N-GNS catalysts.

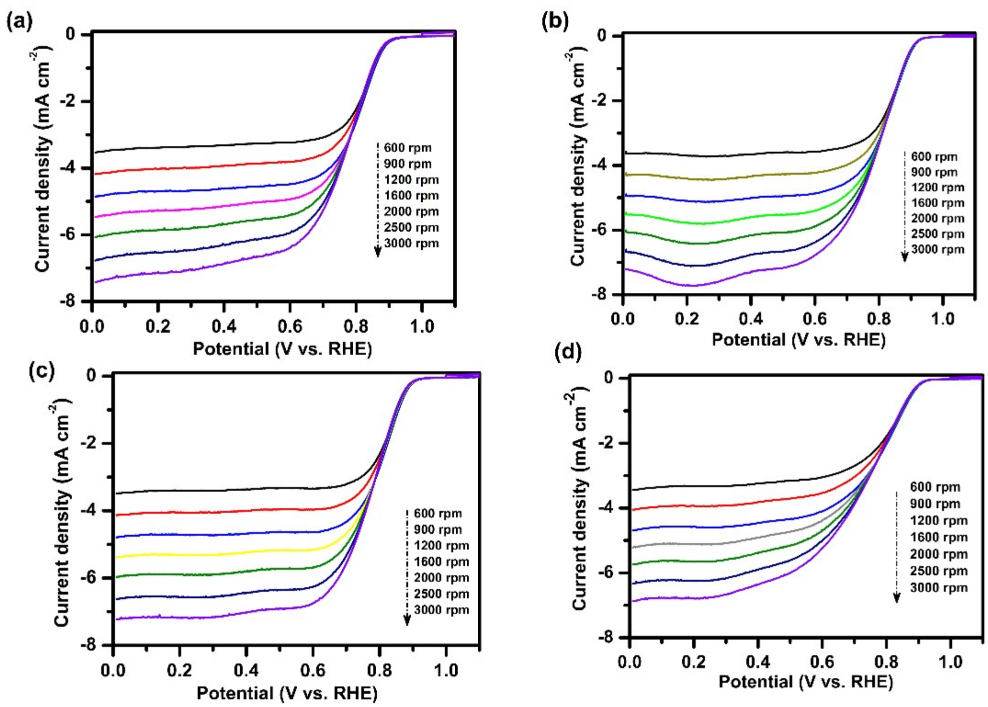

Fig. S8. The ORR polarization curves for (a) Fe-N-GNS, (b) Ni_1@Fe-N-GNS, (c) Ni_2@Fe-N-GNS, and (d) Ni_4@Fe-N-GNS catalysts in O_2-saturated 0.1 M KOH solution at different rotations rates ($\nu = 10$ mV s^{-1}).

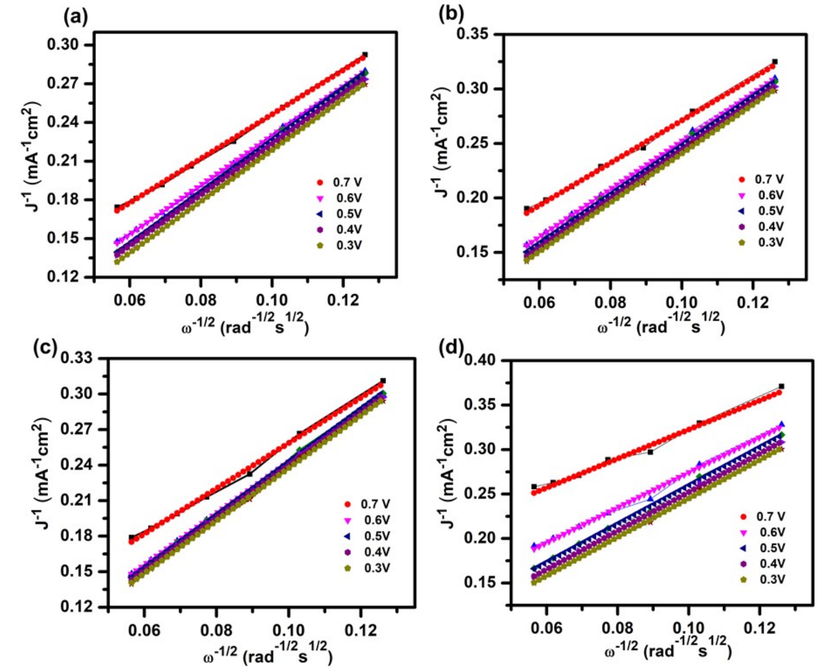

Fig. S9. Koutecky-Levich plots for ORR on (a) Fe-N-GNS. (b) Ni_1@Fe-N-GNS, (c) Ni_2@Fe-N-GNS, and (d) Ni_4@Fe-N-GNS catalysts in O_2-saturated 0.1 M KOH solution at different potentials.

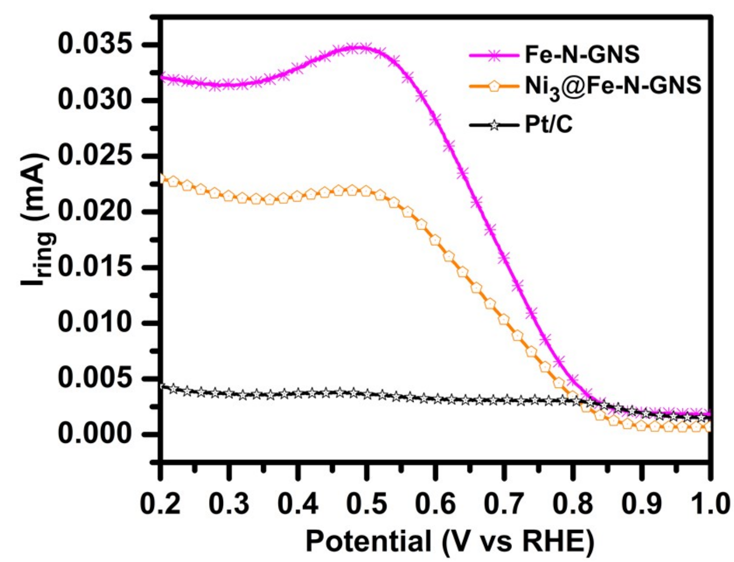

Fig. S10. Ring current of Ni_3@Fe-N-GNS, Fe-N-GNS, and Pt/C catalysts obtained from RRDE test at 1600 rpm.

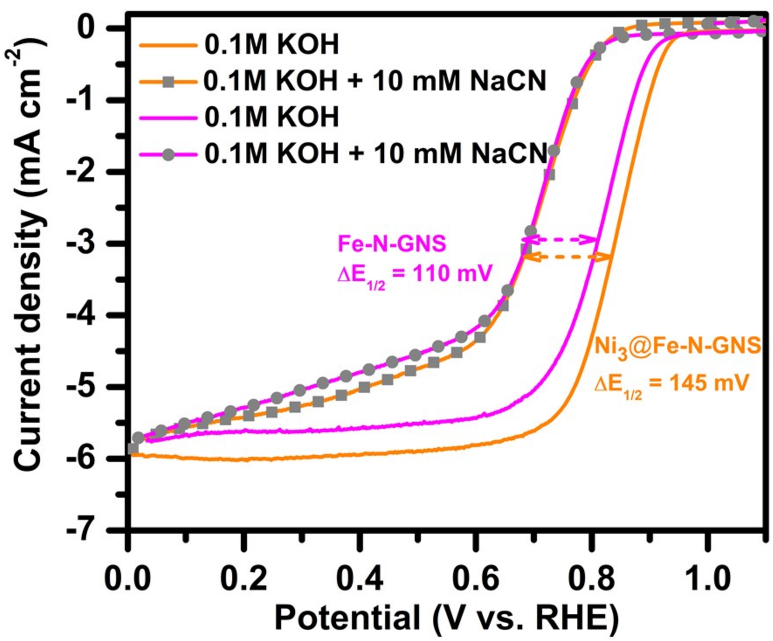

Fig. S11. RDE polarisation curve of Ni_3@Fe-N-GNS and Fe-N-GNS with and without 10mM NacN in O_2-saturated 0.1 M KOH at 1600 rpm

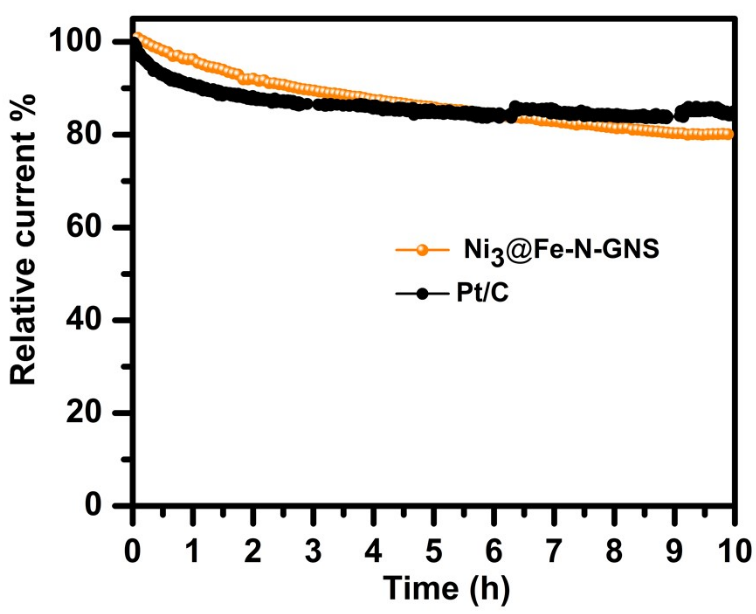

Fig. S12. Chronoamperometric reponse of Ni_3@Fe-N-GNS in O_2-saturated 0.1 M KOH at 1600 rpm.

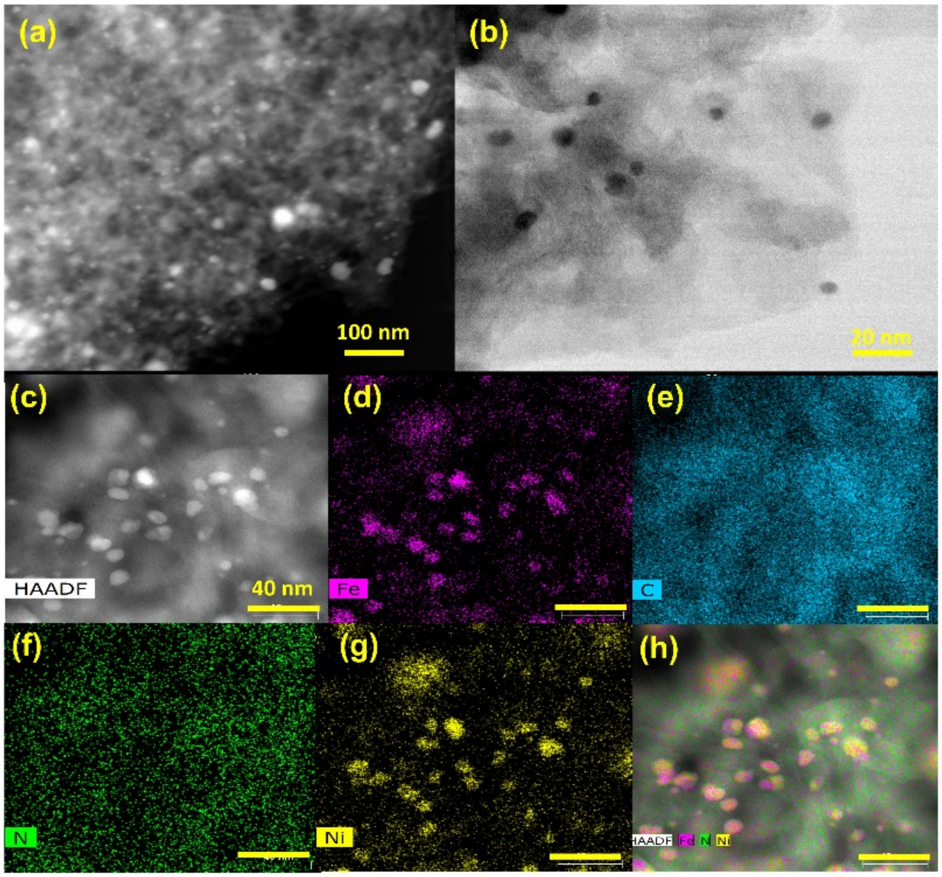

Fig. S13. (a-b) STEM images at different magnifications (c-h) HAADF-STEM image and corresponding elemental maps of Fe, C, N, Ni after (i-t) measurement of Ni_3@Fe-N-GNS.

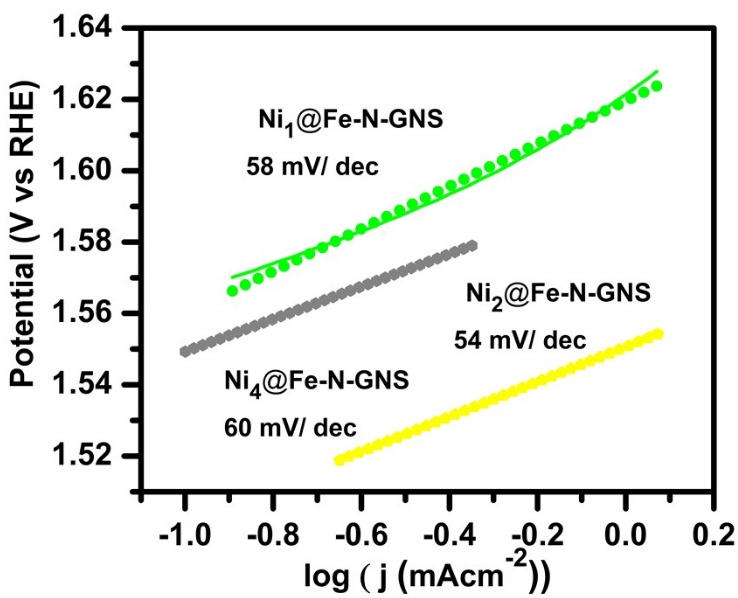

Fig. S14. Tafel plots for OER on the Ni_1@Fe-N-GNS, Ni_2@Fe-N-GNS, and Ni_4@Fe-N-GNS catalysts.

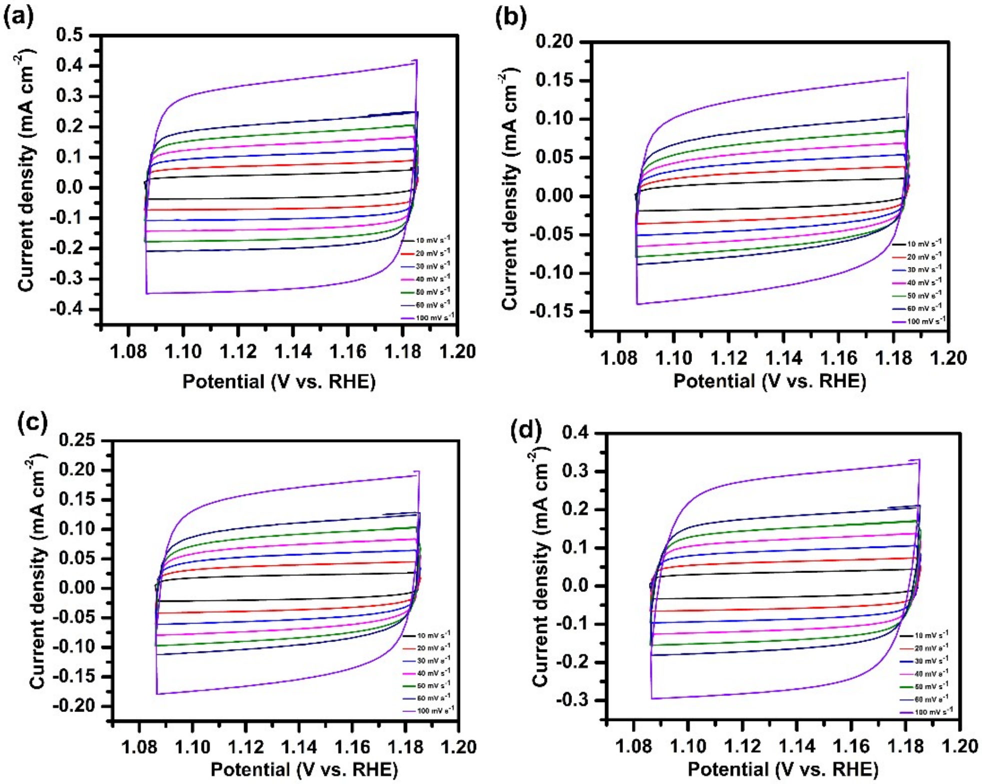

Fig. S15. CV's of the (a) Fe-N-GNS, (b) Ni_1@Fe-N-GNS, (c) Ni_2@Fe-N-GNS, and (d) Ni_4@Fe-N-GNS catalyst materials in Ar-saturated 0.1 M KOH solution at scan rates from 10 to 100 mV s^{-1}.

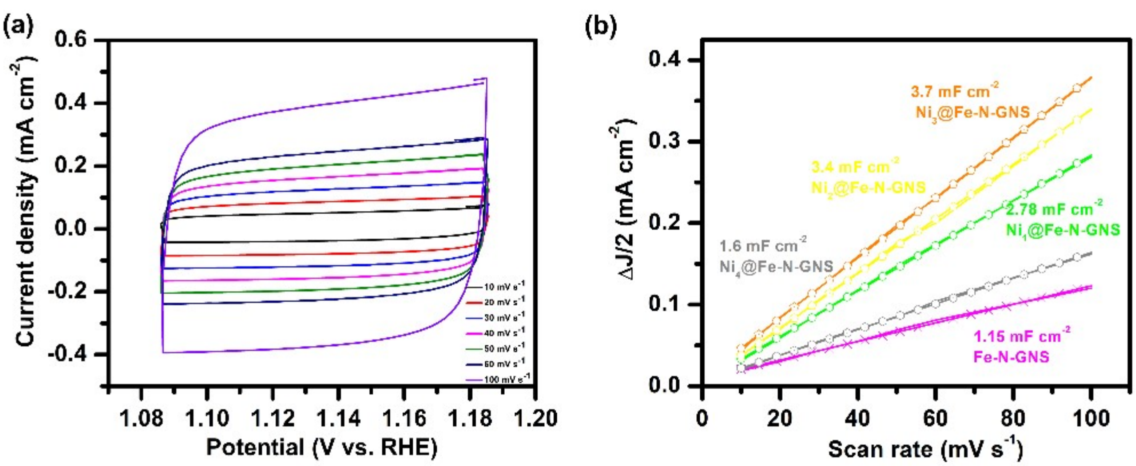

Fig. S16. (a) CV's of Ni_3@Fe-N-GNS catalyst measured in Ar-saturated 0.1 M KOH solution at scan rates from 10 to 100 mV s^{-1}. (b) C_{dl} of all the prepared catalysts.

Table S5: Comparison of the ORR and OER parameters of all the prepared catalysts in 0.1 M KOH.

Catalyst	Loading (mg cm^{-2})	E_{onset} (V) vs RHE (ORR)	$E_{1/2}$ (V) vs RHE (ORR)	E_{10} (V) vs RHE (OER)

Ni_4@Fe-N-GNS	0.2	0.91	0.771	*
Ni_3@Fe-N-GNS	0.2	0.96	0.834	1.65
Ni_2@Fe-N-GNS	0.2	0.92	0.808	*
Ni_1@Fe-N-GNS	0.2	0.92	0.808	1.68
Fe-N-GNS	0.2	0.92	0.807	*
Pt/C	0.1	-	0.838	-
RuO_2	0.1	-	-	1.72

*missing values or the catalyst's OER current density does not reach 10 mA cm^{-2}.

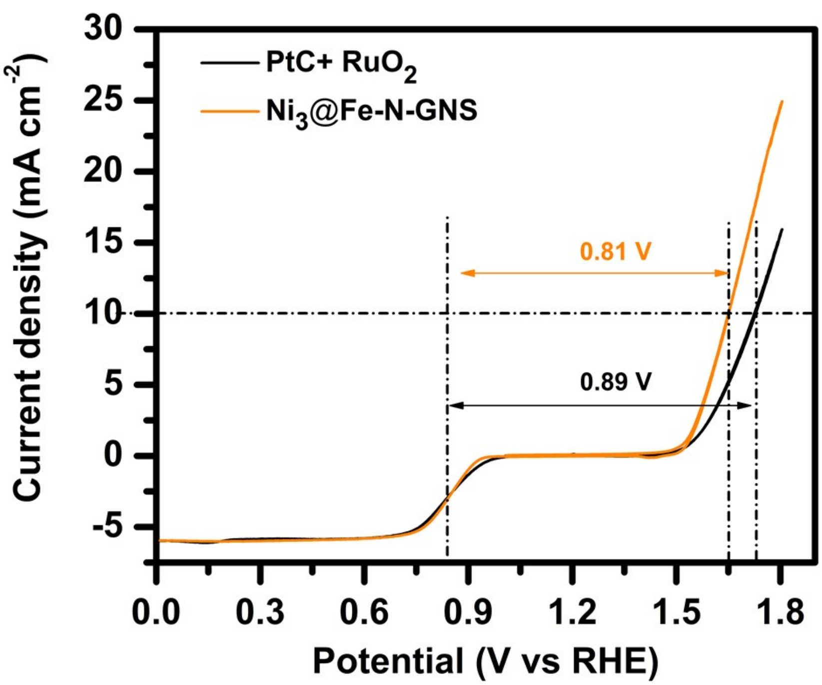

Fig. S17. LSV curves of Ni_3@Fe-N-GNS and Pt/C + RuO_2 catalysts for ORR and OER in 0.1 M KOH.

Table S6. Bifunctional performance comparison of the Ni_3@Fe-N-GNS electrocatalyst with other works.

Catalyst	**$E_{1/2}$ for ORR (V vs. RHE)**	**E_{10} for OER (V vs. RHE) or η for OER**	**ΔE (V)**	**Voltage gap / V**	**Stability / h**	**Ref.**
Ni_3@Fe-N-GNS	0.834	1.65	0.81	0.71	180	This work
Ni0.6Fe0.4	0.75	1.51	0.76	0.96	69	[3]
Ni_3Fe/N-C	0.85	1.56	0.71	0.798	300 @ 2 runs	[4]
Ni_3FeN	0.78	1.588	0.808	0.70	100	[5]
CoNi/BCF	0.80	1.60	0.80	__	60	[6]
Co-NiO NFs	0.79	1.53	0.74	0.72	110	[7]
-NiFePS/CNT@NF	0.88	η = 232 mV	0.623	-	132 @ 3 runs	[8]
NiFe/N-CNT	0.75	η = 290 mV	0.77	0.61	100	[9]

FeNi3@NC	0.86	η = 277 mV	0.65	0.75	30	10
FeCo/Se-CNT	0.9	1.65	0.75	0.878	70	11
FeNi@N-CNT/NCSs	0.84	1.59	0.75	0.73	40	12
CNT@SAC-Co/NCP	0.87	1.61	0.74	0.51	33.6	13
NiFe@N-CFs	0.82	1.53	0.71	0.66	150	14
$Co_{0.7}Fe_{0.3}$@NC2:1-800	0.827	η = 314 mV	-	0.835	60	15
NiFeP/Pi	0.82	1.44	0.62	0.70	100 @ 3 runs	16
NiO/$NiCo_2O_4$	0.73	η = 357 mV	0.86	0.78	175	17

Table S7. The comparisom of Ni_3@Fe-N-GNS based Zn-air battery performance with reported works.

Catalyst	Loading (mg cm^{-2})	OCV (V)	P_{max} (mW cm^{-2})	Specific capacity (mAh g^{-1})	Ref.
Ni_3@Fe-N-GNS	**2**	**1.47**	**171**	**894 @20 mA cm^{-2}**	This work
FePc‖CNTs‖NiCo/CP	0.8	1.44	219.5	748.2 @ 10 mA cm^{-2}	18
Fe/Ni(1:3)-NG	1	1.50	164.1	824.3	19
Fe(Zn)-N-C	1	1.44	193	800@10 mA cm^{-2}	20
Fe,Mn/N–C	0.5	1.40	160.8	902 @ 5 mA cm^{-2}	21
NiFePS/CNT@NF	5	1.41	134.5	737.1 @10 mAcm-2	8
NiCoFeP-HN	10	1.41	109	754 @ 5 mA cm^{-2}	22
Fe/Co–N–C	-	1.52	188	808 @ 10 mA cm^{-2}	23
FeCo-NSC	2	1.51	152.8	782.1@20 mA cm^{-2}	24

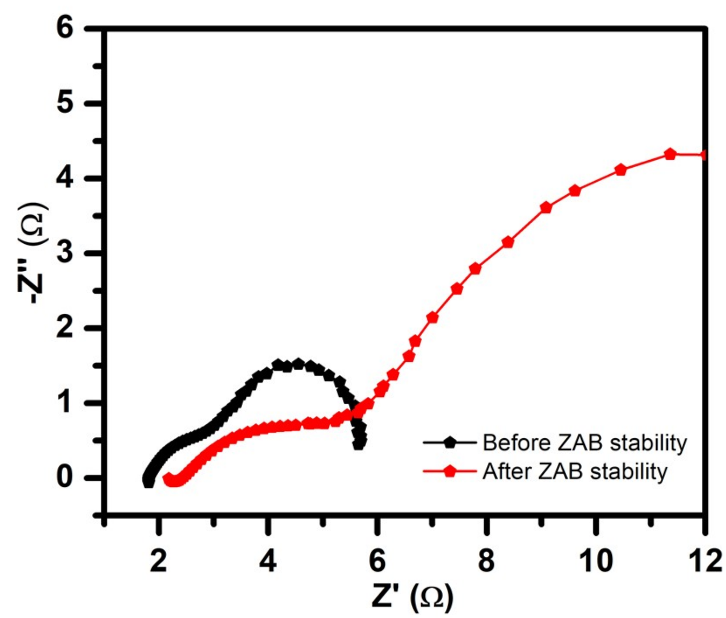

Fig. S18. EIS measurement of Ni_3@Fe-N-GNS catalyst as air cathode in ZAB before and after stability measurement at 1.25 V.

References:

1. A. J. Bard and L. R. Faulkner, *Electrochemical methods: fundamentals and applications*, John Wiley & Sons, 2nd ed. New York, 2001.
2. X. Ge, A. Sumboja, D. Wuu, T. An, B. Li, F. W. T. Goh, T. S. A. Hor, Y. Zong and Z. Liu, *ACS Catalysis*, 2015, **5**, 4643-4667.
3. Y.-y. Li, Q. Zou, Z. Li, D. Xie, Y. Niu, J. Zou, X. Zeng and J. Huang, *Applied Surface Science*, 2022, **572**, 151286.
4. H. Gong, X. Zheng, K. Zeng, B. Yang, X. Liang, L. Li, Y. Tao and R. Yang, *Carbon*, 2021, **174**, 475-483.
5. G. Fu, Z. Cui, Y. Chen, L. Xu, Y. Tang and J. B. Goodenough, *Nano Energy*, 2017, **39**, 77-85.
6. W. Wan, X. Liu, H. Li, X. Peng, D. Xi and J. Luo, *Applied Catalysis B: Environmental*, 2019, **240**, 193-200.
7. G. Fang, J. Gao, J. Lv, H. Jia, H. Li, W. Liu, G. Xie, Z. Chen, Y. Huang, Q. Yuan, X. Liu, X. Lin, S. Sun and H.-J. Qiu, *Applied Catalysis B: Environmental*, 2020, **268**, 118431.
8. B. Liu, S. Wu, G. Chen and Y. Han, *The Journal of Physical Chemistry C*, 2024, **128**, 12346-12354.
9. H. Lei, L. Ma, Q. Wan, Z. Huangfu, S. Tan, Z. Wang and W. Mai, *Nano Energy*, 2022, **104**, 107941.
10. D. Chen, J. Zhu, X. Mu, R. Cheng, W. Li, S. Liu, Z. Pu, C. Lin and S. Mu, *Applied Catalysis B: Environmental*, 2020, **268**, 118729.
11. H. Zhang, M. Zhao, H. Liu, S. Shi, Z. Wang, B. Zhang, L. Song, J. Shang, Y. Yang, C. Ma, L. Zheng, Y. Han and W. Huang, *Nano Letters*, 2021, **21**, 2255-2264.
12. J.-T. Ren, L. Chen, Y.-S. Wang, W.-W. Tian, L.-J. Gao and Z.-Y. Yuan, *ACS Sustainable Chemistry & Engineering*, 2020, **8**, 223-237.
13. J.-C. Li, Y. Meng, L. Zhang, G. Li, Z. Shi, P.-X. Hou, C. Liu, H.-M. Cheng and M. Shao, *Advanced Functional Materials*, 2021, **31**, 2103360.
14. Y. Niu, X. Teng, S. Gong and Z. Chen, *Journal of Materials Chemistry A*, 2020, **8**, 13725-13734.
15. L. Long, H. Liu, J. Jia, Y. Zhang and S. Dong, *Nanoscale*, 2021, **13**, 2609-2617.
16. N. Thakur, M. Kumar, D. Mandal and T. C. Nagaiah, *ACS Applied Materials & Interfaces*, 2021, **13**, 52487-52497.
17. Z. Zhang, X. Liang, J. Li, J. Qian, Y. Liu, S. Yang, Y. Wang, D. Gao and D. Xue, *ACS Applied Materials & Interfaces*, 2020, **12**, 21661-21669.
18. S. Ding, L. He, L. Fang, Y. Zhu, T. Li, Z. Lyu, D. Du, Y. Lin and J.-C. Li, *Advanced Energy Materials*, 2022, **12**, 2202984.
19. Y. Ma, H. Fan, C. Wu, M. Zhang, J. Yu, L. Song, K. Li and J. He, *Carbon*, 2021, **185**, 526-535.
20. Y. Ma, Y. Xiao, Y. Ge, D. Gao, Y. Zhang, Z. Li and Y. Han, *Journal of Materials Chemistry A*, 2024, **12**, 2004-2010.
21. G. Yang, J. Zhu, P. Yuan, Y. Hu, G. Qu, B.-A. Lu, X. Xue, H. Yin, W. Cheng, J. Cheng, W. Xu, J. Li, J. Hu, S. Mu and J.-N. Zhang, *Nature Communications*, 2021, **12**, 1734.
22. B. He, C. Xu, Y. Tang, Y. Qian, H. Liu, Q. Hao and Z. Su, *Journal of Materials Chemistry A*, 2019, **7**, 24964-24972.
23. R. Dun, X. He, J. Huang, W. Wang, l. Yiwei, L. Li, B. Lu, Z. Hua and J. Shi, *Journal of Materials Chemistry A*, 2023, **11**, 5902-5909.
24. Y. Wu, C. Ye, L. Yu, Y. Liu, J. Huang, J. Bi, L. Xue, J. Sun, J. Yang, W. Zhang, X. Wang, P. Xiong and J. Zhu, *Energy Storage Materials*, 2022, **45**, 805-813.